www.rericjournal.ait.ac.th

CFD Modeling of a Downdraft Gasifier with Woodchips used as Feedstock

Charissa Enget* and Kitipong Jaojaruek*,[1]

Abstract – *CFD analysis is a useful tool that can be used to optimize the design of gasifiers. Although plenty of CFD analysis has been performed on fluidized bed gasifiers, little analysis has been performed on the biomass gasification of solid fuels due to the difficulty in modeling the chemical phenomena in the combustion of solids. In order to simplify calculations, previous CFD simulations have modeled fuel beds by creating homogenous beds with uniform spacing or beds with simplified shapes like spherical particles. However, in real experimental conditions, fuel beds are non-homogenous and particle position is randomized. This study aimed to fill the gap of research simulations on realistically modeled fuel beds. In this study, a downdraft gasifier was modeled using cubic woodchips as fuel and air as a gasifying agent. Woodchips were individually placed in the gasifier in random orientation to imitate the positioning of when biomass is fed from the top of a gasifier. CFD analysis was performed on the effect of air flow rate and feedstock properties on air velocity, air trajectory, and average pressure throughout the gasifier. The applications of these analyses were demonstrated in this paper; they include blower size optimization, pressure drop calculation for non-uniform beds, combustion zone range determination, air inlet design, and velocity and pressure profile generation and analysis. An optimal flow rate was chosen based on previous experimentation and results of the optimized flow rate for this gasifier were given in this paper.*

Keywords – *CFD, downdraft gasification, modeling of gasifiers, pressure drop, velocity profile.*

1. INTRODUCTION

Biomass gasification is a thermochemical process which converts raw biomass into combustible products to be used as energy. Biomass is defined as any organic material which is used as a fuel. The most common types of biomass used as fuel are agricultural waste, garbage, landfill gas, alcohol fuels, and wood. Since 2001, the popularity of biomass gasification has continuously risen as the prices of oil have increased and people have searched for a solution to the global climate change crisis [1]. In 2018, global energy consumption increased to 2.1% due to a 3.8% economic growth at purchasing power parity [2]. This trend of increasing energy consumption is due to the bi-directional causality between energy consumption and economic growth. As economies continue to expand globally, energy expenditure is expected to continue increasing [3]. Renewable energy sources like biomass, wind, and solar energy are being looked at globally to provide for this predicted increase. Biomass is considered one of the best options to reduce the global environmental impact because its utilization can theoretically give a near zero net CO_2 emission and it has the potential to reduce waste.

Biomass currently accounts for over 10% of global energy consumption [1], [4]. However, much of this biomass consumption is through the traditional usage of biomass as fuel: direct combustion for heating and cooking processes. Traditional usage of biomass is inefficient and has a negative environmental impact. However, biomass can be converted into useful combustible gases, liquids, and solid fuel through means of thermochemical conversion. Thermochemical conversion is a route used to convert bio-renewable resources into energy dense fuel; its processes include pyrolysis, liquefaction, and gasification. Gasification is a thermochemical process which turns feedstock into combustible and non-combustible gases. The combustible gases produced can be used to power internal combustion engines (ICE) and turbines. Biomass gasification has several advantages as an energy source: biomass is abundantly available, it is less location and climate dependent than other renewable energy sources, it's considered a carbon neutral energy source, and storage and transport of biomass is easy and simple.

There are many different types of gasifiers. These include updraft or counter-current gasifiers, downdraft or co-current gasifiers, cross-draft gasifiers, and fluidized bed gasifiers. Updraft, downdraft, and cross-draft gasifiers contain solid feedstock which rests on a grate and is partially combusted by an oxidizing agent whereas fluidized bed gasifiers suspend solid particles in an oxidizing agent so that the bed acts as a fluid.

Gasification involves four different processes. First, feedstock goes through drying, a process in which moisture content within the feedstock is evaporated. Next, the feedstock enters into the pyrolysis stage. In pyrolysis, oxygen is choked in order to prevent combustion, and high temperatures cause the decomposition of the biomass into valuable chemicals. Then, the feedstock enters the combustion zone where feedstock is partially combusted in order to supply heat to the gasification, drying, and pyrolysis zones. Last, the

*Mechanical Engineering Department, Faculty of Engineering, Kasetsart University, Kamphaeng Saen, Nakhon Pathom 73140, Thailand.

[1]Corresponding author:
Tel: + 66 081 374 2507, Fax: +66 034 355 310.
Email: fengkpj@ku.ac.th.

feedstock enters the gasification zone in which raw materials are transformed into hydrocarbon gases, liquids, and char. These processes and their locations in a downdraft gasifier are shown in Figure 1. The product of gasification, or producer gas, consists of both combustible and non-combustible gases [5]-[7]. Producer gas can be used as fuel directly with internal combustion engines or gas turbines after going through cleaning processes [1], [6].

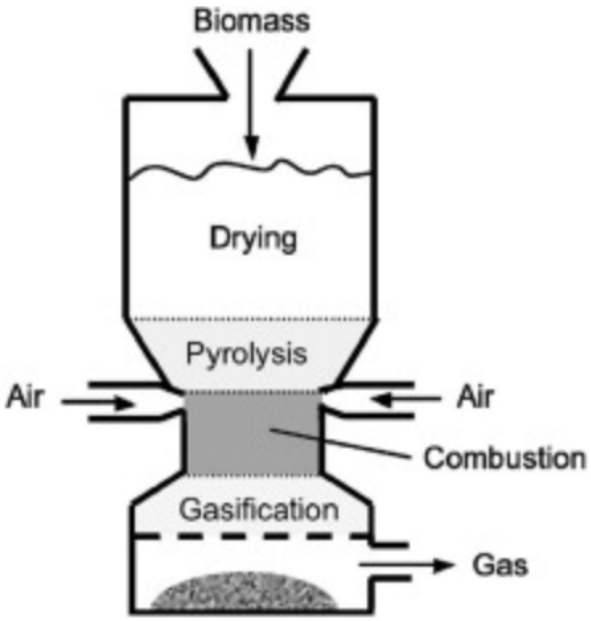

Fig. 1. Schematic of a throated downdraft gasifier [8].

Many parameters must be considered in the design of biomass gasifiers. For example, loose biomass has been known to cause clogging in the throats of downdraft biomass gasifiers. For this reason, Shelke *et al.*, performed experiments on biomass sawdust briquettes to find a method to prevent woodchip clogging. They discovered that biomass shape and size can be modified to utilize various biomass in a downdraft gasifier without modification of the gasifier [9]. Next, the tar content of biomass must be considered in gasifier design. Tar buildup can cause problems in engines or turbines using producer gas due to condensation, polymerization, and formation of tar aerosols. Rubio *et al.*, achieved a 74% reduction in tar, 27% increase in efficiency, and 30% increment in HHV by implementing a shaking grate mechanism in a downdraft gasifier [10]. Ash is also an important parameter to consider, as ash can cause slagging problems, erosion and corrosion of equipment, and ash deposition which can lead to equipment failure, decreased efficiency, and high cleaning costs. Tar content, particle size, particle density, and ash content are all important in optimizing the design of gasifiers for successful and safe experimentation. Mathematical modeling is often used to optimize gasifier designs before construction in order to save on experimental cost and time. It is particularly useful for scaling up laboratory-scale apparatus to both demonstration-scale and commercial-scale gasifiers. Generally, gasification mathematical models are separated into two categories: lump analysis and finite computation analysis. Lump analysis treats the gasification system as a whole where finite computation analysis models the system by dividing it into many small elements.

Currently, extensive computational fluid dynamics (CFD) models have been created to study fluidized bed gasifiers. However, research involving CFD modeling of gasifiers using solid biofuels is limited. This is because there is great difficulty in modeling the chemical phenomena of combustion of solid biomass with CFD, therefore a comprehensive model of solid biomass gasification has not yet been developed.

CFD is a branch of fluid dynamics which analyzes fluid flow through the use of numerical analysis and data structures. This type of modeling falls under the finite computation analysis category. Numerical computation is performed through the use of computers which allows CFD to solve some of the world's most incredibly complex problems. These problems include aerodynamics, combustion analysis, industrial system design, weather analysis, and engine analysis. CFD analysis begins by defining the physical geometry of a structure using computer aided design (CAD). The volume of the fluid to be analysed is then divided into discrete cells comprised of elements and nodes, a process called meshing. Meshes must be fine enough to capture the areas of fluid flow of interest in sufficient detail required for the experiment. However, fine meshes come at the cost of greater computational complexity, so meshing must be done efficiently. Next in the CFD analysis process, the physical model is defined by the experimental parameters being measured:

equations of fluid motion, radiation, enthalpy, conservation, etc. These equations are then calculated at the nodes defined in the meshing process. Next, boundary conditions are defined at the surfaces of the fluid domain. Finally, the simulation begins and equations are solved iteratively as steady-state or transient flow, which is defined by the user. The results of the calculations are processed after the calculation with post-processing software.

CFD and mathematical modeling are useful tools in optimizing material usage, design parameters, experimental procedures, and time usage for various applications. For example, Kongkapisuth *et al.*, performed CFD analysis of a wind turbine using the k-ε turbulence model which was found useful for determining the effect of velocity and the direction of wind flow on the free spinning speed of several wind turbines [11]. Khan *et al.*, explored the thermal and fluid dynamic characteristics of six pin fin heat exchangers through the CFD analysis of their pressure, temperature, and velocity profiles and determined that elliptical pin fins have the best overall performance [12]. Dejtrakulwong *et al.*, modeled a downdraft gasifier by modeling the four zones of gasification as separate entities and using the preceding zone as an input to the next. Their results gave accurate predictions for composition gases, the temperature of those zones, the effects of the moisture ratio, and the equivalence ratio which were useful to optimize the gasifier design through selection of the reactor dimension. [5] Silva *et al.*, modeled the combustion of biomass in a furnace by releasing volatile gases into two sections of the grate, one where water was already vaporized and one where moisture content in biomass was still present. This model proved to be an efficient tool for the optimization of biomass combustion and for predicting emissions of CO and CO_2 [13]. Jaojaruek *et al.*, developed a mathematical model by deriving energy and mass conversion principles from thermochemical principles for the whole length of a downdraft gasifier. It was determined useful for gasifier design, gas output rate, and the estimation of gas output composition [6]. Kumar *et al.*, developed a CFD model of biomass gasification in which they used a volatile break-up approach for the combustion portion of the gasification model. It was deemed useful for studying the effect of the equivalence ratio on gasifier temperature and output as well as the syngas production of varying biomass feedstock [14]. In all of these, modeling was determined helpful due to its effectiveness in saving time, reducing costs, and optimizing apparatus design.

Currently, extensive computational fluid dynamics (CFD) models have been created to study fluidized bed gasifiers. However, research involving CFD modeling of gasifiers using solid biofuels is limited. This is because there is great difficulty in modeling the chemical phenomena of combustion of solid biomass with CFD, therefore a comprehensive model of solid biomass gasification has not yet been developed. Given that most CFD modeling focuses on fluidized bed gasification, it would be helpful to develop a model of the gasification of solid biomass. In current literature where the gasification of solid biomass is modeled, fuel beds have homogenous spacing and sizing or feedstock is given simplified shapes like spheres for simplicity of calculation. Therefore, this model designed randomly oriented feedstock of cubic woodchips to create a realistic experimental conditions of gasification in a CFD simulation to fill this gap in research. The pressure drop in gasifier beds of solid biomass is typically modeled through empirical correlations which assume particle size to be homogenous, or pressure is assumed constant to simplify this complication. This model aimed to create a method to accurately measure the pressure drop with uniform biomass of random orientation which cannot be modelled with empirical correlations. Next, velocity profiles of gasifiers are most often modeled in fluidized beds where airflow obstruction by biomass is not present, or modeled in beds with uniform particle-size distribution and bed voidage. This model aimed to create a more realistic velocity profile within a biomass gasifier of woodchips to give more accurate calculations of equivalence ratio, better gasifier design through air nozzle placement, and measurement and control of the combustion zone. A downdraft gasifier model and simulation was designed with ANSYS CFX® with the aim of investigating airflow and pressure within a reactor to gain valuable information on the effects of reactor design and woodchip sizing.

2. METHODOLOGY

2.1 Gasifier Geometry and Design

A downdraft gasifier was designed according to the reactor used by Jaojaruek *et al.* In this research, single-stage and two-stage air supply experiments were performed to determine the effects on producer gas due to air supply variance. The reactor simulated in these experiments was designed after the single-stage air supply experiments and therefore only contained air inlet nozzles at the combustion zone [15].

The details of this gasifier can be seen in Figure 2. Starting from the bottom, the base of the gasifier was designed with a diameter of 375 mm which extends to a height of 1500 mm. Above the base of the gasifier, one fuel outlet of 75 mm diameter was placed at a height of 162 mm. Above this, a metal grate spanning the diameter of the gasifier was punctured with holes of 20 mm diameter and placed 300 mm above the base of the gasifier. Large amounts of bed voidage were noticed in previous experiments when woodchips were dropped into a reactor. Therefore, the voids were replicated in this CFD model. Cubic woodchips of volume $(65\ mm)^3$ were placed on top of the grate and filled up to the throat of the gasifier. Woodchips in this design were placed one-by-one in random orientation on top of each other to simulate realistic positioning of biomass feedstock being fed from the top and dropped into the gasifier. Next, four air inlets of 30 mm diameter were placed equidistantly around the circumference of the gasifier at a height of 515 mm above the base. The gasifier stood at a total height of 2100 mm.

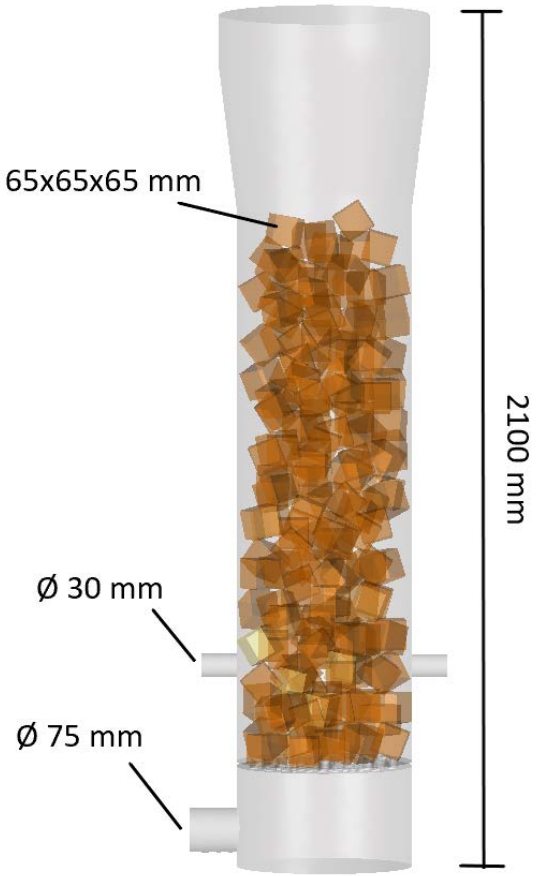

Fig. 2. Downdraft gasifier model with woodchips as biomass feedstock.

2.2 Model Description

The governing transport equations included instantaneous equations of momentum, mass, and energy conservation. Because turbulent flow was modeled in the gasifier, these equations are needed for use as inputs in turbulent equations in ANSYS CFX®.

The continuity equation:

$$\frac{\partial \rho}{\partial t} + \nabla(\rho \boldsymbol{U}) = 0 \tag{1}$$

The momentum equations:

$$\frac{\partial(\rho \boldsymbol{U})}{\partial t} + \nabla \cdot (\rho \boldsymbol{U} \otimes \boldsymbol{U}) = -\nabla p + \nabla \cdot \tau + \boldsymbol{S}_M \tag{2}$$

where the stress tensor, τ, is related to the strain rate by:

$$\tau = \mu(\nabla \boldsymbol{U} + (\nabla \boldsymbol{U})^T - \frac{2}{3}\delta \nabla \cdot \boldsymbol{U}) \tag{3}$$

The total energy equation:

$$\frac{\partial(\rho h_{tot})}{\partial t} - \frac{\partial p}{\partial t} + \nabla \cdot (\rho \boldsymbol{U} h_{tot}) = \nabla \cdot (\lambda \nabla T) + \nabla \cdot (\boldsymbol{U} \cdot \tau) + \boldsymbol{U} \cdot \boldsymbol{S}_M + \boldsymbol{S}_E \tag{4}$$

where $\nabla \cdot (\boldsymbol{U} \cdot \tau)$ is the work due to viscous stresses and $\boldsymbol{U} \cdot \boldsymbol{S}_M$ is the work due to external momentum sources.

Transport equations must be modeled as a closed system and therefore required equations of state for density and enthalpy. Air was assumed to behave as an ideal gas in the gasifier. Therefore, ideal gas equations of state were used in this simulation.

$$\rho = \frac{w p_{abs}}{R_o T} \tag{5}$$

$$\mathbb{d}h = c_p \mathbb{d}T \tag{6}$$

$$c_p = c_p(T) \tag{7}$$

where R_o= *8.314 J / (mol· K),* w is the molecular weight, and p_{abs} is the absolute pressure.

The Reynolds Averaged Navier-Stokes (RANS) Equations were used to solve transport equations for turbulence models. Equations (1)-(4) involve fluctuating components, therefore they must be averaged for use as inputs into RANS equations. The turbulence kinetic energy, k, and the turbulence eddy dissipation, ε, were introduced to the RANS equations to calculate the Reynolds stresses.

$$\frac{\partial(\rho k)}{\partial t} + \frac{\partial}{\partial x_j}(\rho U_j k) = \frac{\partial}{\partial x_j}\left[\left(\mu + \frac{\mu_t}{\sigma_k}\right)\frac{\partial k}{\partial x_j}\right] + P_k - \rho\varepsilon + P_{kb} \tag{8}$$

$$\frac{\partial(\rho\varepsilon)}{\partial t}+\frac{\partial}{\partial x_j}\left[\left(\mu+\frac{\mu_t}{\sigma_\varepsilon}\right)\frac{\partial\varepsilon}{\partial x_j}\right]+\frac{\varepsilon}{k}(C_{\varepsilon1}P_k-C_{\varepsilon2}\rho\varepsilon+C_{\varepsilon1}P_{\varepsilon b}) \quad (9)$$

where $C_{\varepsilon1}$, $C_{\varepsilon2}$, σ_k, and σ_ε are all constants. [16]

2.3 Theoretical Equivalence Ratio

The equivalence ratio (ER) is the ratio of the actual air-fuel ratio in the gasifier to the stoichiometric air-fuel ratio. ER is only used in situations where air supply is choked, like in a gasifier. ER must be less than one, otherwise complete combustion will occur which will prevent gasification processes from occurring.

In order to calculate the ER, first the stoichiometric requirement *b* for oxygen must be calculated per unit *a* feedstock of composition $C_xH_yO_z$..

Equation 10 must then be balanced with the following relations.

$$ax = c \quad (11)$$

$$ay = 2d \quad (12)$$

$$az + 2b = 2c + d \quad (13)$$

After finding the value *b*, the stoichiometric requirement of air could be found. Equation 14 assumes air to be composed of 21% oxygen and 79% nitrogen for simplicity.

$$Air = 0.21O_2 + 0.79N_2 \quad (14)$$

$$b\ mol\ O_2/0.21\ O_2 = Air_{stoi}\ mol \quad (15)$$

By knowing that the molar mass of air is 29 g/mol, the ideal mass of air could be calculated. Subsequently, knowing the molar mass of C (12.010 g/mol), H (1.008 g/mol), and O (15.999 g/mol), the ideal mass of fuel could then be calculated as well.

$$m_{air} = Air_{stoi} * 29\ g/mol \quad (16)$$

$$m_{fuel} = a * ((x\ mol\ C) * (12.010\ g/mol\ C) + (y\ mol\ H) * (1.008\ g/mol\ H) + (z\ mol\ O) * (15.999\ g\ /\ mol\ O)) \quad (17)$$

Then, the stoichiometric air fuel ratio could be found.

$$(A/F)_{stoi} = m_{air}/m_{fuel} \quad (18)$$

Finally, the theoretical ER (ϕ) was found by dividing the actual amount of air supplied with the stoichiometric air.

$$\phi = \frac{Air_{actual}}{Air_{stoi}} \quad (19)$$

2.4 Meshing

Meshing is a process used to split a structure into smaller components in order to calculate parameters of a structure with greater accuracy. In meshing, a finite number of grid points within a structure called nodes is created. At these nodes, governing equations are solved numerically for the parameters desired. The governing equations solved at the nodes in this model were described in Section 2.2. The finite volume method is used to solve these equations. The greater the density of the meshing, the greater the accuracy in solving the problems. However, greater accuracy comes at the cost of greater difficulty in solving the equations. Therefore, meshes must be created in a balance with enough density to capture the most important details, but with a low enough density where the software is able to solve the equations in a timely manner.

The gasifier was meshed with 9055632 nodes and 5993614 elements. The total volume of the mesh was 0.172 m^3 which is shown in Figure 3. This gasifier had a complicated structure due to the structure of the grate and the biomass woodchips. Intricate meshing was required to accurately capture the details of the airflow and pressure in these regions.

A face sizing metric was given to the walls of the gasifier containing the woodchips, excluding the throat of the gasifier and above. This face sizing was necessary to prevent the space between the woodchips and the gasifier from inflating too quickly and missing features. This face sizing parameter was given a uniform element size and the intricate detail of that mesh is displayed in Figure 4.

The grate was given its own specific mesh due to its complicated structure. The diameter of the grate was designed with many 20 mm holes creating an intricate surface with many edges, 105 faces, and irregular shapes which required a great attention of detail for accurate modeling. In order to capture these details, a specific face meshing was created for this structure with a smaller element sizing than the woodchips.

The gasifier is a very complicated structure due to the woodchips modeled inside of it. The mass of woodchips creates a mass with many corners, edges, and 974 faces which all required detailed meshing in order to capture the intricacies during air flow simulations for accurate results. The woodchip faces were given an element size of 4e-03 m.

An inflation sizing was put on the entire body of the gasifier to create an efficient mesh. The growth ratio was set at 1.2 for medium growth rate in mesh sizing with a smooth transition.

2.5 Boundary Setup and Experimental Parameters

The working fluid chosen as the oxidizing agent for these experiments was air as an ideal gas. Air was set to a temperature of 40˚C, initialized at a high turbulence with intensity equal to 10% and relative pressure of 100 Pa at the outlet nozzle, and a reference pressure of 1 atm. Cubic woodchips were set up inside the gasifier as a wall with a sand roughness of 40 microns [17]. Fluid flow was modeled with the standard k-ε model to simulate turbulent flow inside the reactor. For stable solutions, relaxation factors were adjusted and all of the variables converged to 10e-5. Air was set to enter the gasifier at four air nozzle inlets of 30 mm diameter with cumulative flow rates of 100, 150, 200, 250, 300, 350, and 400 LPM and to exit at the outlet nozzle. In the

comparative experiments, each of the four air nozzles were given an individual airflow meter so that each nozzle gave equal airflow to a good degree of accuracy. Therefore, airflow in the CFD model was supplied to each air nozzle in equal flow rates to mimic experimental conditions. Velocity and pressure data were calculated and subsequently put into post-processing software for data analysis. Data was then put into contours, graphs, and vectors for proper visualization and analysis. The seven flow rates were compared and a final optimized flow rate was chosen and displayed. The results of this analysis are shown in the following section.

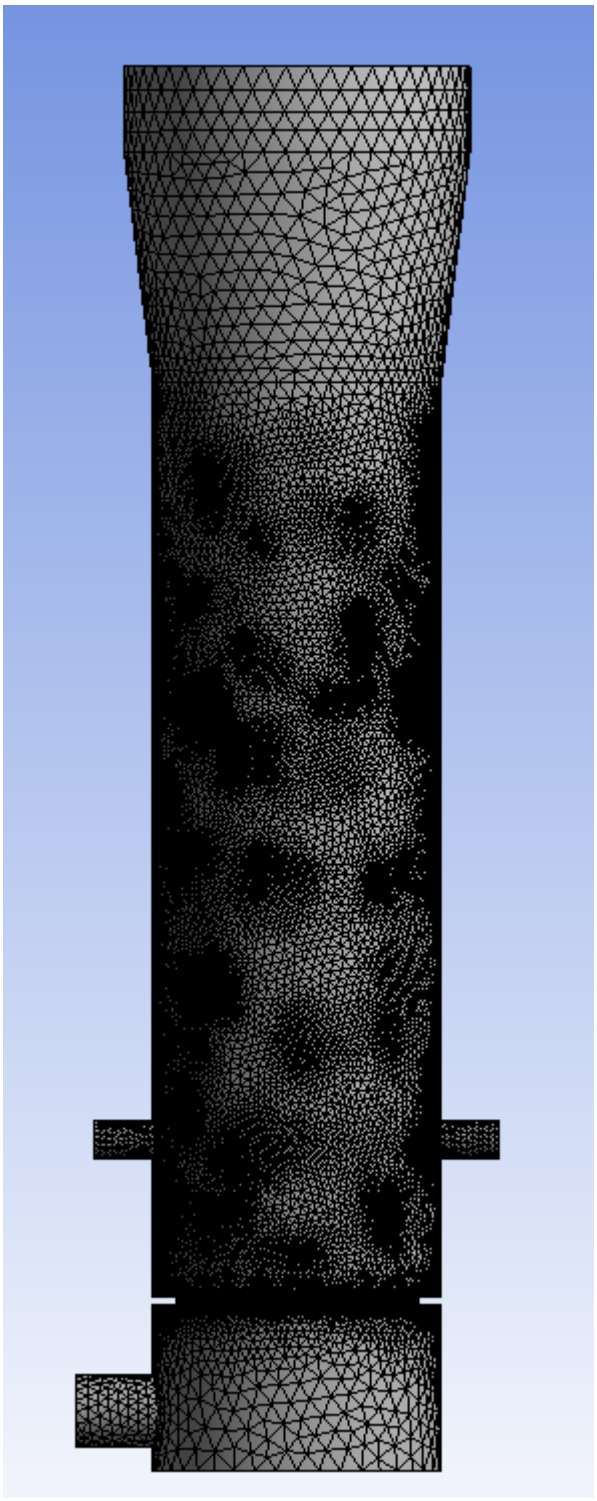

Fig. 3. Mesh of the entire body of the reactor.

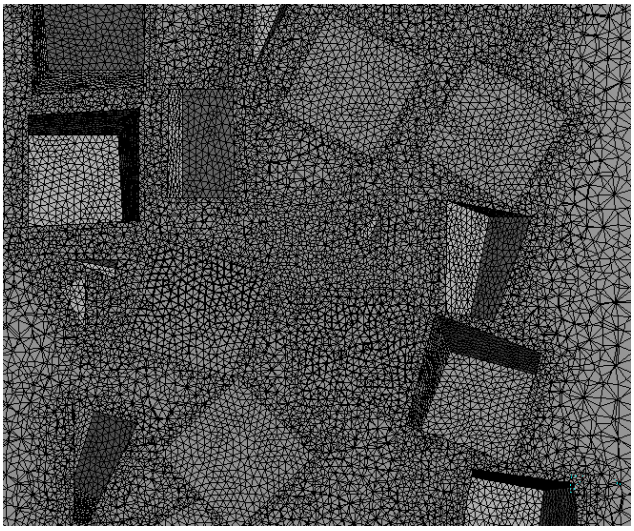

Fig. 4. Close-up meshing of the inside of the reactor.

3. RESULTS AND DISCUSSION

3.1. Comparison and Evaluation of Velocity Profiles

The velocity profiles were measured at flow rates ranging from 100 to 400 LPM at 50 LPM increments. In Figure 5, a velocity contour was created at the cross section of the gasifier at the height of the center of the air inlets for all seven flow rates. Velocities were measured on a global color scale for comparison and ranged from 0.0 to 0.9 m/s. This type of analysis is useful to show the effect of the shape, roughness, and particle size of the feedstock on airflow within a gasifier. Also, biomass obstruction of airflow can cause air to be unable to travel throughout the diameter of the gasifier. The top and bottom nozzles shown in Figure 5 were completely obstructed, but the side nozzles allowed air to reach the center despite blockages. Therefore, four air nozzles were deemed a suitable amount for this size and shape of feedstock in a gasifier of this size. This method of analysis is useful for determining the necessary number of air inlets for different sizes and shapes of biomass feedstock to create homogenous combustion.

In Figure 6, the instantaneous velocity of the center point of the plane shown in Figure 5 was measured. The results were plotted as the velocity of the air inlets vs. two y-axes: the magnitude of the velocity at the center point of the plane and the percentage decrease in velocity from the inlets to the center points. The particle size, roughness, and shape greatly impacts airflow reach. As shown by Figure 6, the center velocity increased from 0.021 at 100 LPM to 0.122 at 400 LPM, an increase of 60%. This type of analysis is useful to predict whether homogenous combustion can be attained throughout the biomass bed. If air only reaches the outside of the biomass, combustion will be distorted and biomass will burn insufficiently in the combustion zone. Distorted combustion affects the temperature profile negatively which in turn, has negative effects on producer gas production and HHV. So, an airflow optimization where homogenous combustion can occur can be obtained with this analysis.

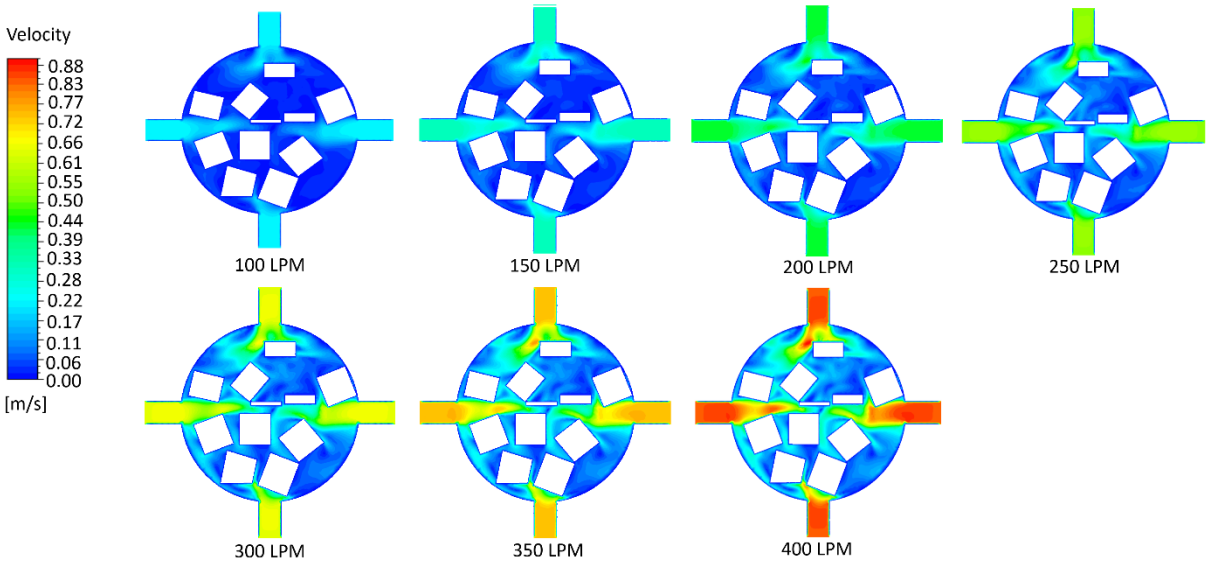

Fig. 5. Velocity contour at the cross section of air inlets in the gasifier.

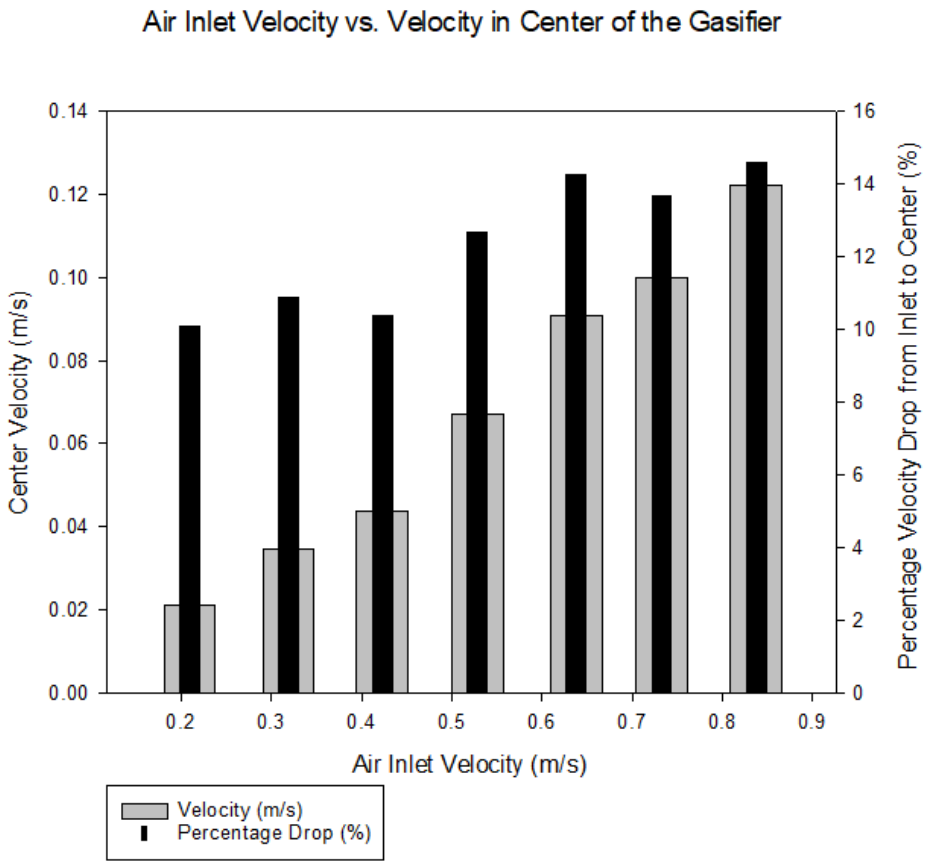

Fig. 6. Air inlet velocity vs. the velocity in the center of the cross section of the air inlets in the gasifier and the percentage velocity drop from the inlets to the center.

In Figure 7, the global velocity vector profile was taken at the mid-plane of the gasifier. The velocity of the fluid inside the gasifier ranged from 0 to 1.142 m/s and each colored velocity profile was scaled on this global range. As flowrates increased from 100 LPM to 400 LPM, the combustion zone expanded to greater heights and higher flowrates reached the center of the feedstock. From 100 LPM to 400 LPM, the height of the combustion zone increased by about 60-80 mm. A larger combustion zone produces higher temperature and higher producer gas production rates. The airflow rate also affects the gas composition. Increased airflow rate was found to increase hydrogen and decrease carbon monoxide and carbon dioxide output [18], [19]. Depending on the amount of heat generation and gas product output desired, this analysis could be used for blower size selection for optimal combustion rates based on the air velocity profile for solid biomass.

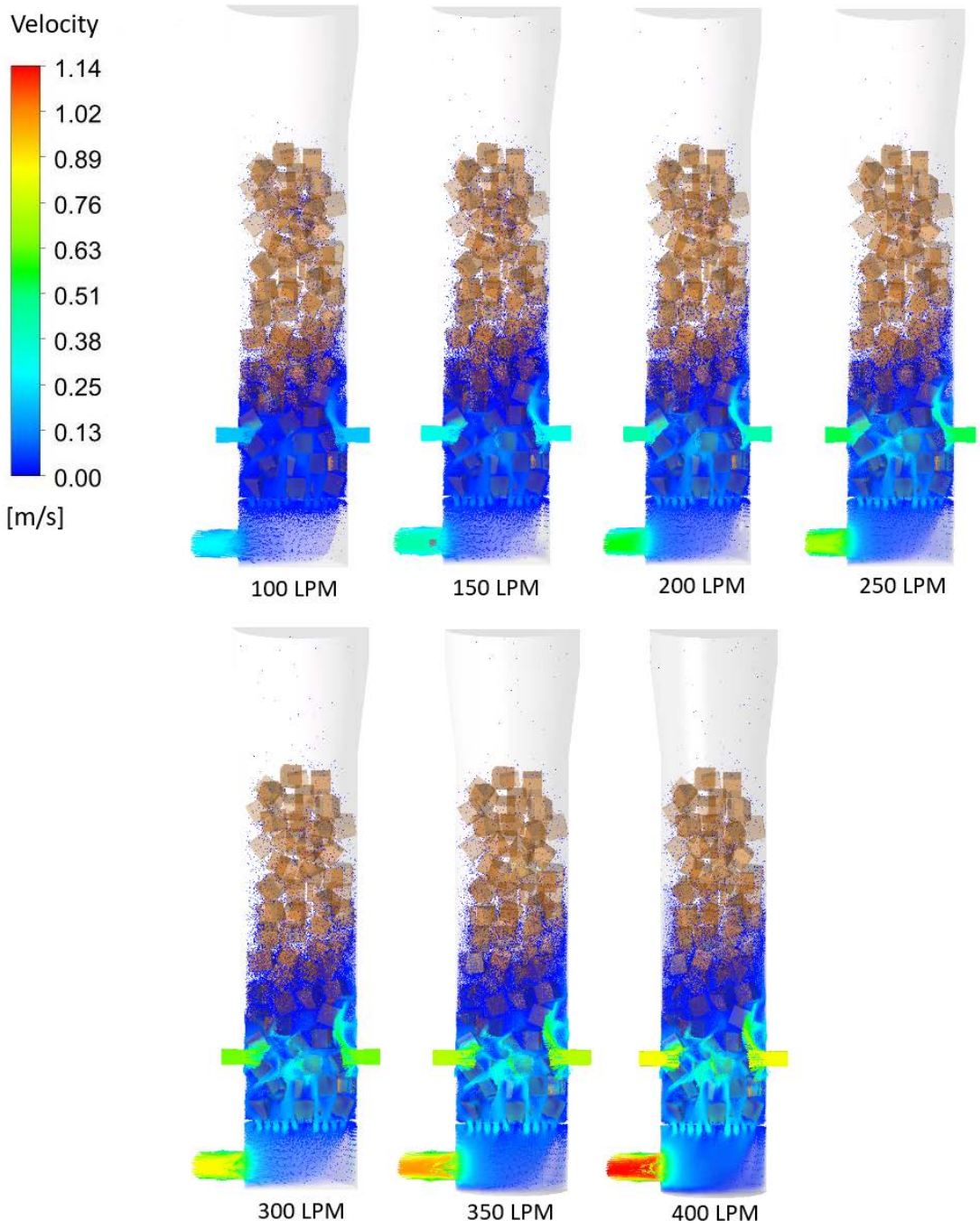

Fig. 7. Air velocity vectors of gasifiers at air inlet flowrates increasing from 100 to 400 LPM.

In Figure 8, the air velocity was measured at three separate planes for air flow rates of 100, 200, and 300 LPM. These planes consisted of the cross section at the center of the fuel outlet, the plane located at the center point between the air inlet and fuel outlet, and the cross section of the air inlets. These were located at heights of 0.15, 0.33, and 0.51 m respectively. Air velocities were consistently highest at the fuel outlet due to a high volume of air converging at the outlet in order to exit the reactor. Higher flow rates correlated with higher air velocities in all planes of the reactor, as shown in Figure 8. Velocities were highest in areas where feedstock was most dense, because air was forced to converge and flow through small spaces.

In Figure 9, the air velocity was measured at sixteen locations starting from the center of the fuel outlet and ending at the height of the biomass feedstock. The global velocity was averaged over a plane for the width of the gasifier at planes were spaced apart by .09 m. The heights of those planes are labeled in the figure. This analysis shows that the average velocity converges to zero at the top of the reactor for all flow rates. This analysis is also useful for finding the exact height where the combustion zone ends. In this case, airflow was absent above 0.96 m for all flow rates which is useful for temperature profile estimation.

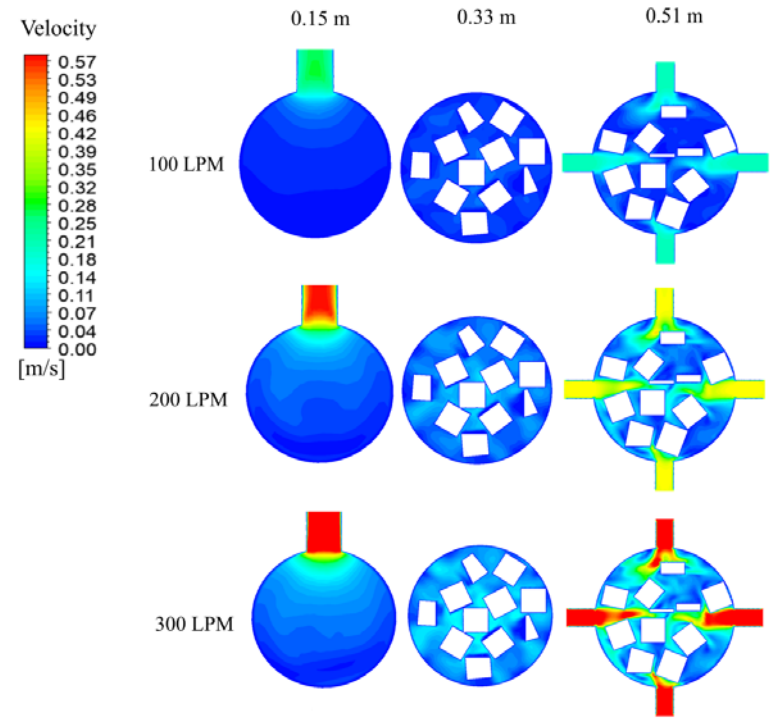

Fig. 8. Velocity contour at the cross-section at three heights in the gasifier at three different flowrates.

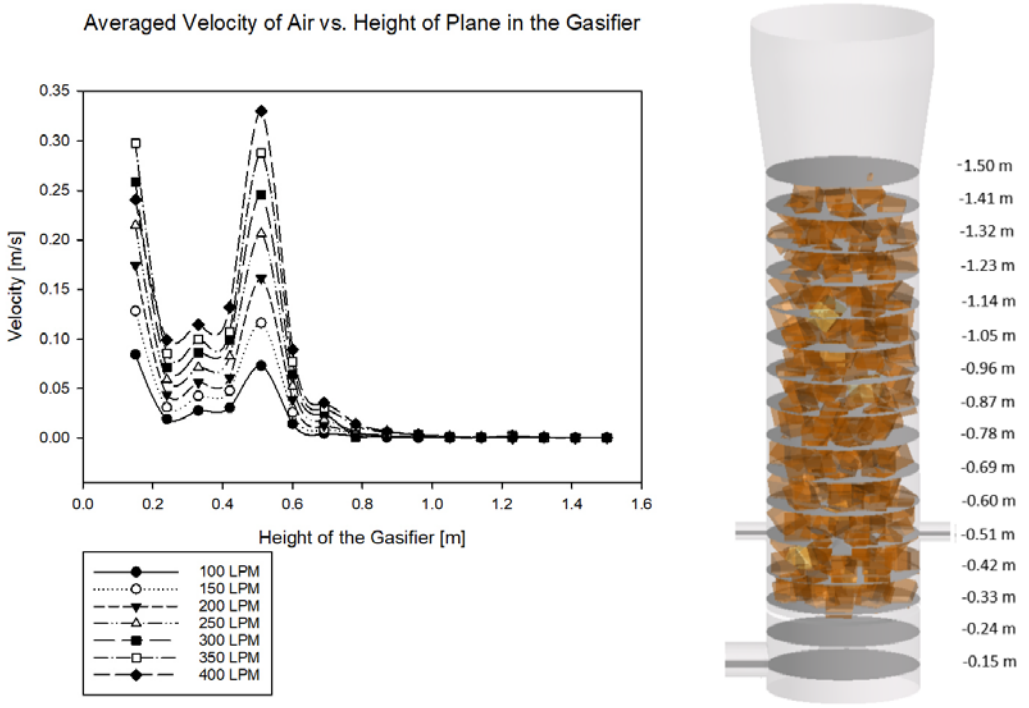

Fig. 9. Average velocity of a plane vs. height of plane in the gasifier.

Figure 9 also offers an insight on the effect of air velocity on combustion within a gasifier when compared to results from Jaojaruek *et al.* [6]. This study measured temperatures throughout the reactor and plotted them according to their height above the grate which is shown in Figure 10. This figure shows that the temperature profile steepens above the combustion zone for higher air supply. It also shows that the highest temperature for all flow rates occurs directly at the air nozzles which correlates with the combustion zone, and higher air flow rates correlated with higher combustion temperatures in this study. Figure 9 shows that the highest average air velocity at the air supply location correlated with the highest temperature at the air supply location for all of the flow rates shown in Figure 10.

3.2 Comparison and Evaluation of Pressure Profiles

In the same way the velocity profile was measured in Figure 9, an average pressure profile was calculated starting from the fuel outlet to the height of the

woodchips in order to determine the pressure gradient and the pressure drop across the gasifier. Figure 11 describes the pressure gradient throughout this area as a function of height inside the gasifier for seven air flow rates. Higher air flow rates caused higher pressure drops overall, however, above a height of 0.69 m, pressure remained homogenous throughout the gasifier for each flow rate. Pressure differences were greatest between the air inlets and the fuel outlet. The visualization that Figure 11 provides is helpful to see how certain shapes, features, and irregularities of different feedstock affected the pressure drop within a gasifier. When gasifiers are combined with internal combustion (IC) engines, pressure drops have been shown to decrease volumetric efficiency which subsequently causes the amount of exit gas to be reduced, decreasing the IC engine power output [1]. Pressure drop has also been shown to be augmented by the gasification of biomass with small particle-size [7]. Therefore, CFD simulation is a valuable tool to predict pressure drop for different size biomass particles and to optimize gasification producer gas and power output.

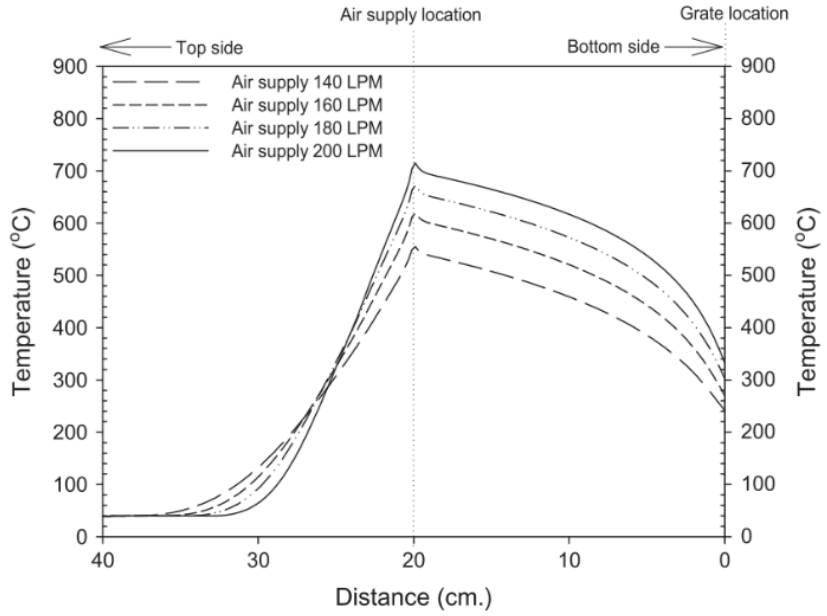

Fig. 10. Experimental temperature profile of the gasifier at varying air supply, [6].

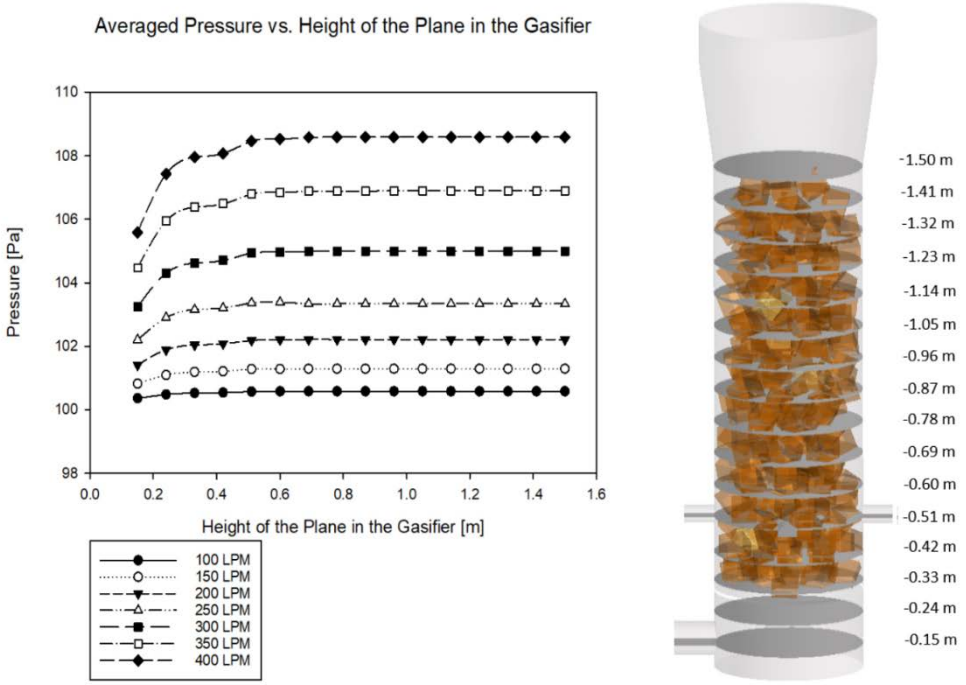

Fig. 11. Average pressure of a plane vs. height of plane in the gasifier.

In Figure 12, a contour of the pressure profile at the cross section of the center of the air inlets was taken. These pressure profiles were put on a global scale and placed on a single graph for visual comparison. It can be seen clearly that higher air flow rate was congruent with higher pressure. The figure shows that pressure buildup was caused by airflow colliding into solid biomass feedstock. The highest points of pressure were located directly next to air inlets where airflow was strongest and hit an obstruction. This visualization is helpful to see how certain shapes, features, and irregularities of different feedstock will affect the pressure distribution within a gasifier. Blower designs are prominently based off of air flow, static pressure, and power requirements. Therefore, results in Figure 12 and Figure 5 are valuable tools to determine the necessary blower size in the design of a downdraft gasifier.

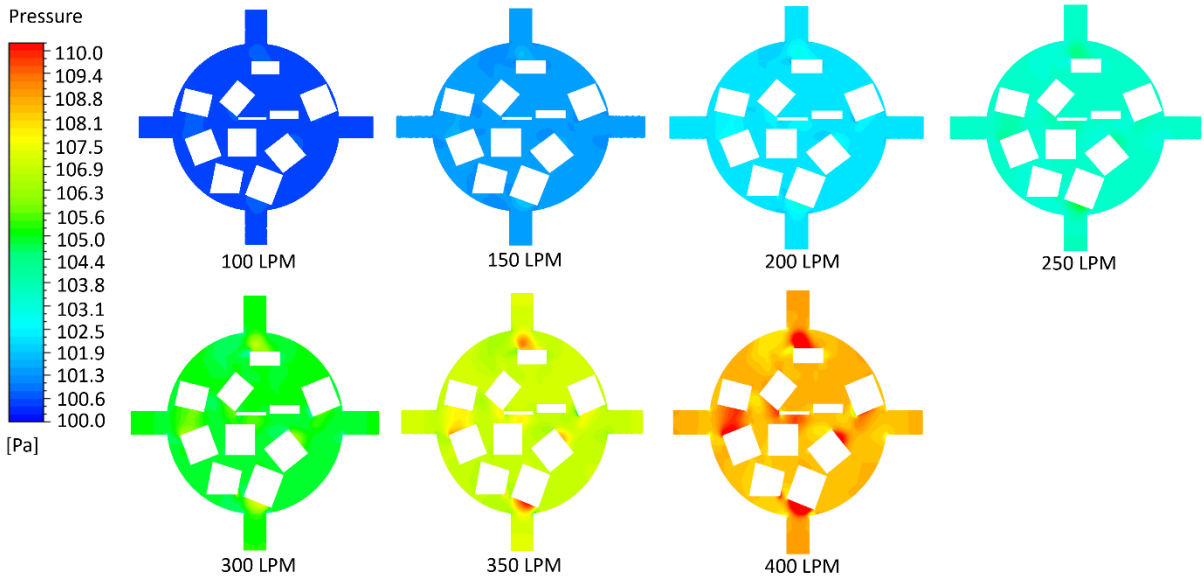

Fig. 12. Comparison of pressure for air inlet flow rates of 100 to 400 LPM.

Furthermore, pressure gradient is important for mathematical modeling of gasifiers. While many models have assumed constant pressure in gasifier biomass beds, loose bioresidues tend to have lower permeability which means pressure drop within these models cannot be dismissed. For uniform shapes like cubes and spheres, empirical correlations for pressure distribution can be calculated. For example, Luckos *et al.*, used developed a method using the Ergun equation to predict pressure drops in homogenous beds of fine particles. But, their model was unable to describe the particle-size distribution in the bed of a commercial Sasol-Lurgi gasifier and therefore could not accurately predict its pressure drop. [20] Wider particle size distribution also causes lower bed voidage which could be modeled accurately with the methods described in this paper. Beds with wide particle size distributions have been shown to have higher pressure drops than beds with lower particle size distributions and greater pressure differences throughout the bed [21]. This is shown in Figure 13, where pressure contours were taken at three different heights between the air inlet and fuel outlet at four air inlet flow rates ranging from 100 to 400 LPM. It is clear from these contours that non-homogenous pressure is more apparent in gasifiers with higher air inlet flow rates, as color contrasts were much greater in beds with higher air inlet flow rates than beds with lower air inlet flowrates. The pressure hardly changed at any height in the gasifier at the flowrate of 100 LPM but the pressure change at differing heights as well as within the same plane were quite drastic at 400 LPM.

Most biomass is typically not uniform, and an accurate method to model non-uniform biomass beds as well as calculate the pressure drop would be valuable. Simulation of many types of irregular biomass with varying bed voidage is possible with this type of CFD model which cannot be calculated with empirical correlations presently.

3.3 Selection of Optimal Flowrate

As mentioned previously, this gasifier design was based on the work of Jaojaruek *et al.* The height of the reactor, diameter and placement of the air inlets and fuel outlet, and the feedstock used all closely resemble his apparatus. In their study, the tar content and HHV of gas based on different air flow rates was investigated for a single-stage and two-stage gasification process. The model used in this study is based solely on the single-stage experiments.

Jaojaruek *et al.*, found that single stage gasifiers operated most efficiently at an equivalence ratio of about 0.42, as shown by Figure 14. At equivalence ratios above or below this value, the HHV of producer gas saw a decline [15].

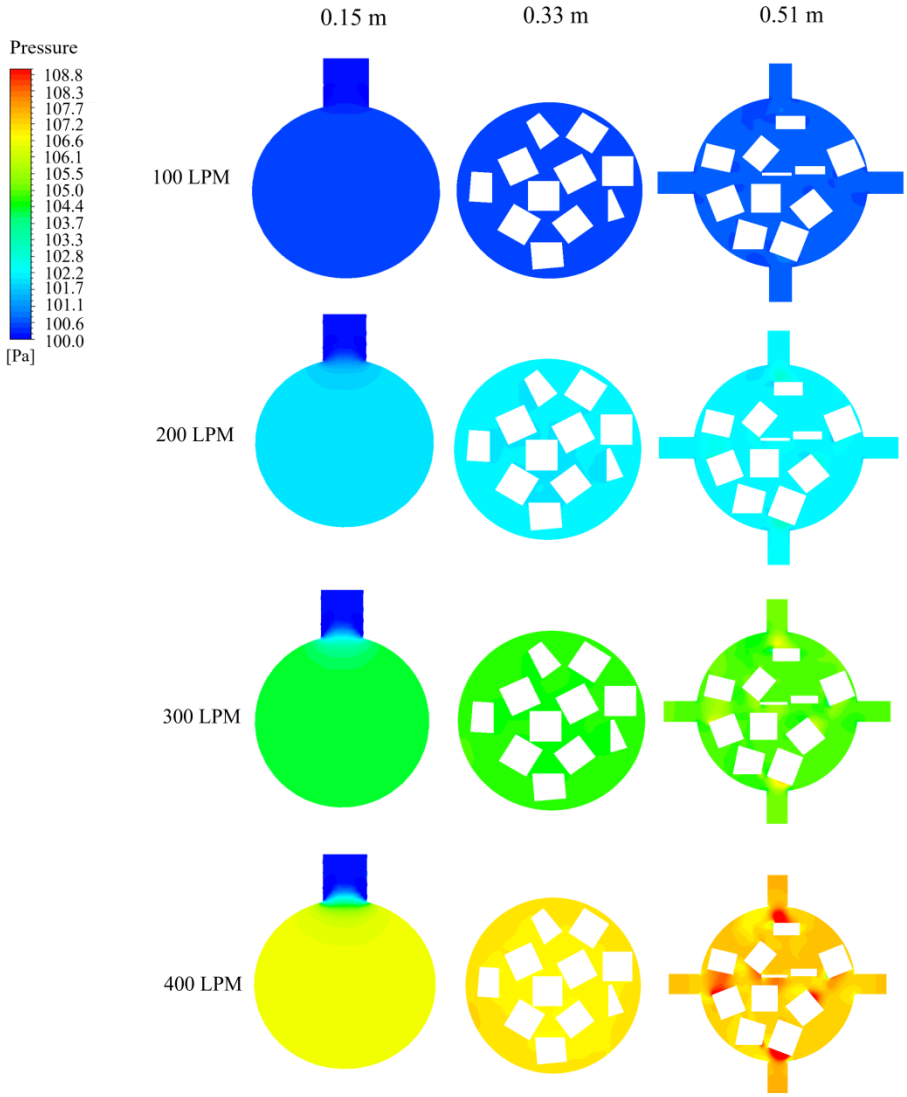

Fig. 13. Comparison of pressure contours for three planes ranging between the air inlet and fuel outlet for four flow rates.

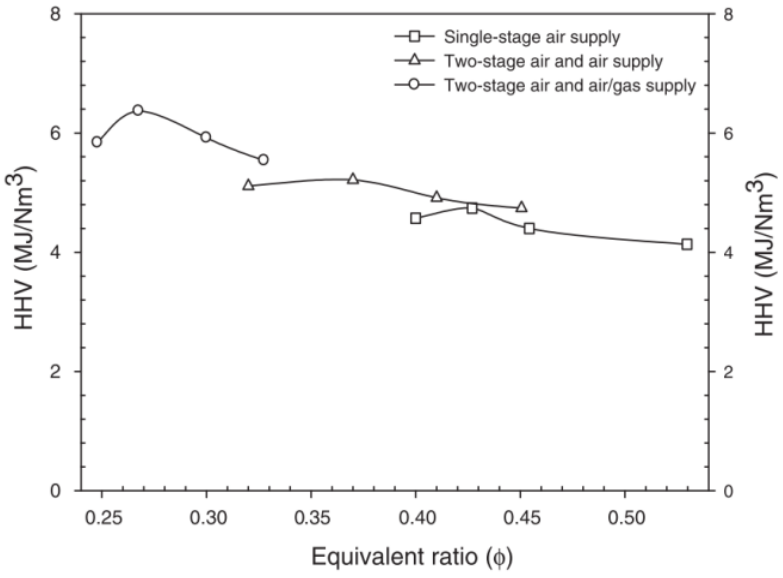

Fig. 14. Equivalent ratio vs. HHV of producer gas for single-stage and two-stage air supply [15].

Although higher flow rates have been proven to provide more expansive combustion zones, higher tar cracking, and more gas output, the HHV value of the gas is the most important parameter to be optimized. The combustibility of the producer gas is of prime importance for use in turbines and internal combustion engines. The equivalence ratio of 0.42 produced the producer gas with the highest HHV for a single-stage air supply gasifier in their experiments. This ER corresponded to a flow rate of 200 LPM in the designed reactor. Therefore, 200 LPM was chosen as the optimized flow rate to be shown in this study. Figure 15 shows the velocity vector profile at a cross section cut halfway through the reactor.

Velocities in the global vector velocity profile in Figure 15 ranged from 0 to 0.58 m/s. Knowing the equivalence ratio, an in depth analysis of the exact airflow trajectory and velocity could allow for a greater understanding of the relationship between the equivalence ratio and combustion zone homogeneity and depth.

In Figure 16, velocities in the velocity contour of the plane measured at the air inlets ranged from 0 to 0.52 m/s. This confirmed that four air inlets were a sufficient amount to produce homogenous combustion throughout the center of biomass feedstock of this size and shape at 200 LPM.

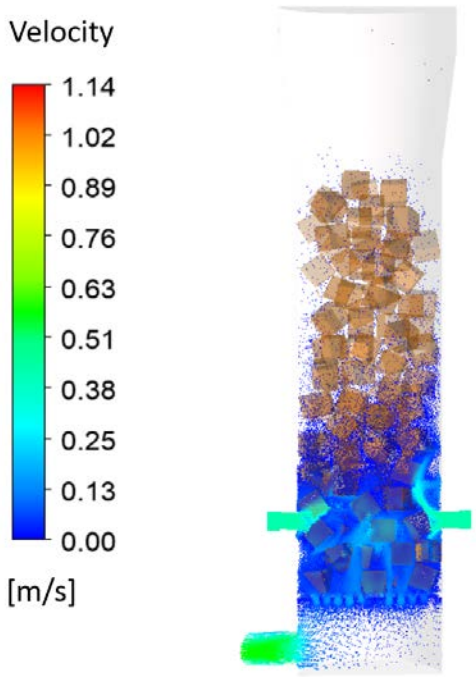

Fig. 15. Vector velocity profile at 200 LPM.

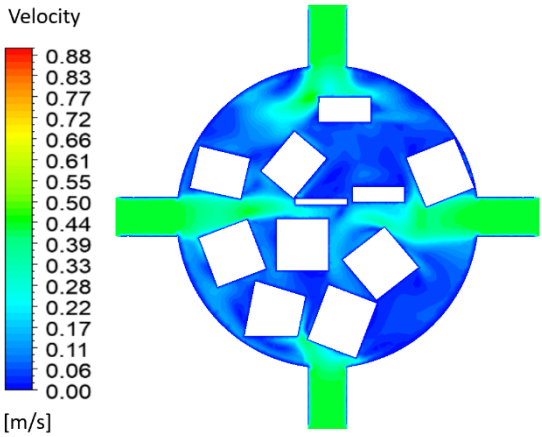

Fig. 16. Velocity contour at cross section of air inlets in the gasifier at 200 LPM.

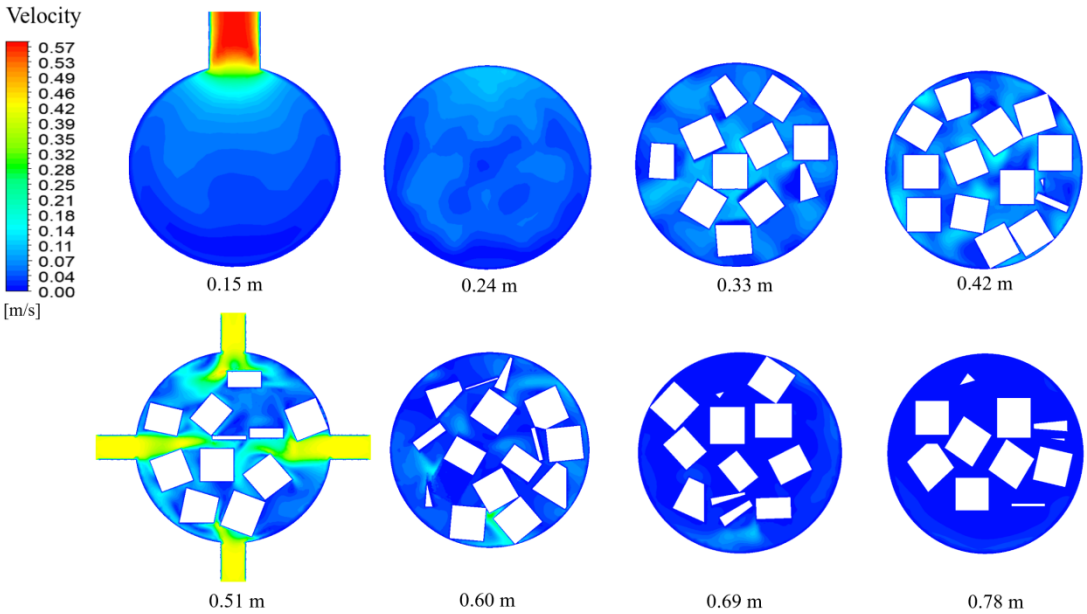

Fig. 17. Velocity contour at 8 different cross sections at ascending heights in the gasifier at 200 LPM.

In Figure 17, velocities were measured at eight planes ranging from heights of 0.15 m to 0.78 m. Velocities ranged from 0 to 0.6 m/s for all planes with air velocity peaking at the outlet. Planes were not shown above 0.78 m since Figure 9 showed that at above the height of 0.69, air velocities converged to zero for all air inlet flow rates. Feedstock affected air velocity by creating higher flow rates in areas with higher feedstock density due to airflow being forced through smaller areas. The denser the section of the gasifier, the higher the flow rate. Moreover, planes in closest proximity to the air inlets and fuel outlet had the highest velocities.

Next, pressures in the plane pressure contour in Figure 18 ranged from 100 to 103.7 Pa. This analysis was helpful in visualizing pressure irregularities in the bed due to biomass feedstock as well as average bed voidage.

Last of all, in Figure 19, pressure contours were measured at eight planes ranging from heights of 0.15 m to 0.78 m. Planes above the height of 0.69 m remained at a static pressure due to homogenous air pressure with little airflow in the top of the gasifier, which was shown in Figure 11. Air pressure peaked in small areas at the air inlets where airflow collided with feedstock. However, average air pressure was highest at the top of the reactor, at a value of around 102.3 Pa. The total pressure drop for the airflow simulation at 200 LPM was 0.77 Pa. The above parameters of velocity and pressure represented in Figures 15-19 are also important for estimating the correct blower sizing, expansion of the combustion zone, pressure drop, and combustion zone homogeneity for this gasifier at this flow rate. The calculation of these parameters is very useful for optimization of gasifier and experimental design.

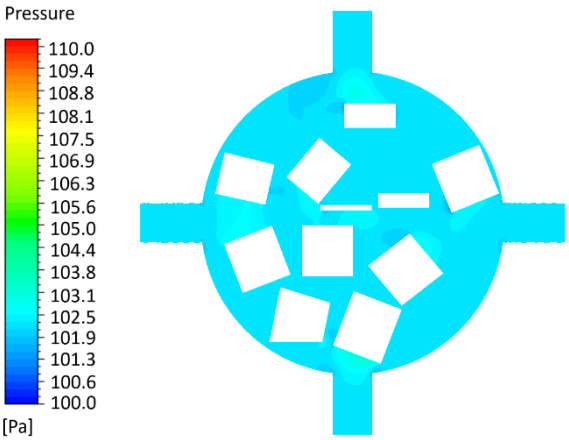

Fig. 18. Pressure contour measured at cross section of air inlets in the gasifier.

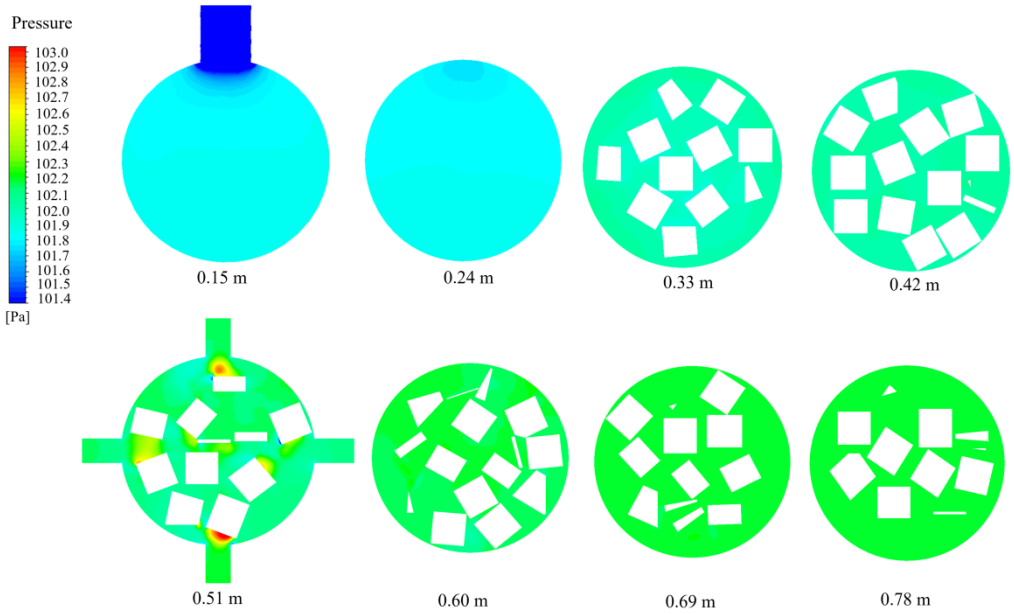

Fig. 19. Pressure contour at 8 different cross sections at ascending heights in the gasifier at 200 LPM.

3.4 Model Validation

The pressure drop was measured at the air inlet and the fuel outlet corresponding to heights of 0.51 m and 0.15 m on the reactor, respectively. The pressure drop was recorded for seven flow rates and compared with experimental values in Figure 20.

Experimental values showed good agreement with the model. CFD model values were ranged within 20-30% of experimental pressure values. This is explained by the surface of the woodchips having uniform shape and roughness in the CFD model which differs from experimental conditions. The degree of difference between the model and real biomass cannot yet be resolved, and therefore cannot be perfected. This lead to the CFD pressure drop having values lower than the experiments. However, model results were reliably in the range 20-30% lower. Therefore, this model was deemed to be a reliable method to calculate pressure profiles and air velocity profiles within the gasifier.

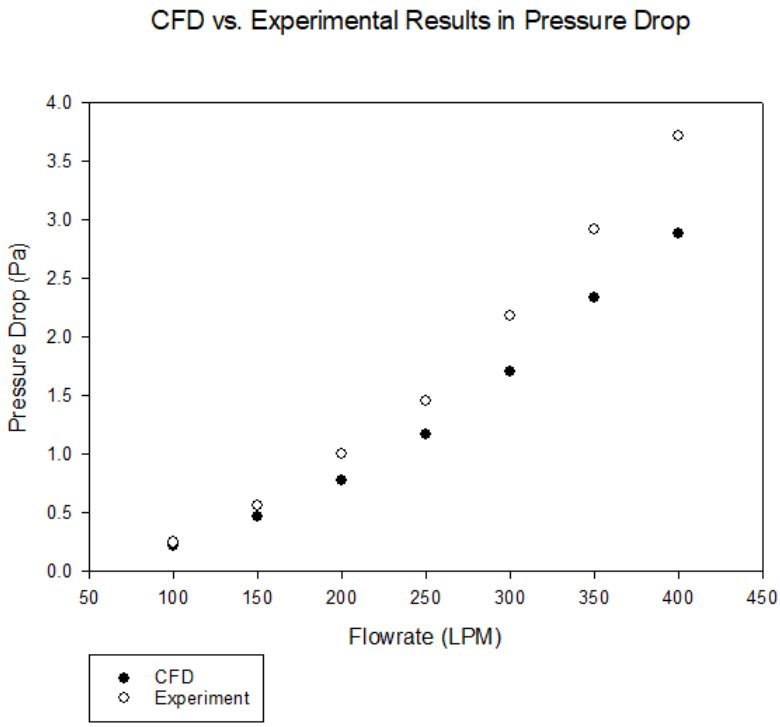

Fig. 20. Measured pressure drop between the air inlet and fuel outlet for CFD and experimental values.

4. CONCLUSION

In this study, the pressure and velocity profiles were modeled with ANSYS CFX® for a gasifier at seven different flow rates ranging from 100 to 400 LPM. It was found that CFD analysis was useful for analyzing pressure buildup in gasifiers with loose biomass feedstock and calculating the pressure drop where empirical correlations cannot be used. CFD analysis was also found to be useful for optimizing the number of air inlets required for airflow to reach the center of the gasifier to induce homogenous combustion. Airflow profiles were useful for approximating the expanse of the combustion zone based on flow rate. Both pressure and velocity profiles were found to be useful for preliminary estimates of blower sizing. Higher air supply flow rates corresponded to higher average pressure, higher pressure drops, higher temperature, and higher average velocity. Although higher velocity airflow at the inlets allowed for greater airflow throughout the gasifier, previous research has found that an equivalence ratio higher or lower than 0.42 causes a decrease in the HHV of producer gas. Therefore, 200 LPM was chosen as the optimal flow rate for this gasifier, since it corresponded to an ER of 0.42, and the results of that optimized simulation were displayed. The model was validated with experimental values of pressure drop and was shown to be an accurate method for calculating velocity and pressure profiles.

ACKNOWLEDGEMENT

The authors would like to express their gratitude to the Mechanical Engineering Department, Faculty of Engineering, Kasetsart University Kamphaeng Saen for their support through their research fund. Their support is the reason this study was accomplished and without it, this research would not have been possible.

NOMENCLATURE

Dimensions are given in fundamental magnitudes of length (L), mass (M), time (T), and temperature (Θ).

Symbol	Description	Dimensions/ Value
$(A/F)_{stoi}$	stoichiometric air-fuel ratio	
Air_{stoi}	stoichiometric air	
$C_{\varepsilon 1}$	k-ε turbulence model constant	1.44
$C_{\varepsilon 2}$	k-ε turbulence model constant	1.92
h	thermodynamic enthalpy	L^2T^{-2}
k	turbulence kinetic energy per unit mass	L^2T^{-2}
m_{air}	ideal mass of air for stoichiometric combustion	M
m_{fuel}	ideal mass of fuel for stoichiometric combustion	M
p	Pressure	$ML^{-1}T^{-2}$
P_k	turbulent production due to viscous forces	
P_{kb}	buoyancy force	
$P_{\varepsilon b}$	buoyancy force	

R_o	universal gas constant	$L^2T^{-2}\Theta^{-1}$, 8314.5
$\boldsymbol{S}_E$	energy source	$ML^{-1}T^{-3}$
$\boldsymbol{S}_M$	momentum source	$ML^{-2}T^{-2}$
t	time	T
T	temperature	
U	velocity magnitude	LT^{-1}
$\boldsymbol{U}$	vector of flow velocity, $\mathbf{U}_{x,y,z}$	LT^{-1}
w	molecular weight	

Greek Letters

δ	identity matrix	
ε	turbulence eddy dissipation	
λ	thermal conductivity	$MLT^{-3}\Theta^{-1}$
μ	molecular (dynamic) viscosity	$ML^{-1}T^{-1}$
μ_t	turbulent viscosity	$ML^{-1}T^{-1}$
ρ	density	ML^{-3}
σ_k	turbulence model constant for the k equation	1.0
σ_ε	*k-ε* turbulence model constant	1.3
τ	stress	$ML^{-1}T^{-2}$

Mathematical Operator

∇	Vector, $\nabla = \left[\frac{\partial}{\partial x}, \frac{\partial}{\partial y}, \frac{\partial}{\partial z}\right]$
⊗	Dyadic Operator
𝕕	Exact differential, $\mathbb{d}z(x,y) = M\,dx + N\,dy$

Subscripts

abs	absolute
j	component
tot	total

REFERENCES

[1] Sikarwar V., Zhao M., Clough P., Yao J., Zhong X., Memon M. Z., Shah N., Anthony E. and Fennell P., 2016. *An overview of advances in biomass gasification* (Vol. 9).

[2] Enerdata, *Global Energy Trends-2019 Edition.* 2019: Grenoble, France.

[3] Marques L., Fuinhas J., and Marques A., 2015. On the global energy consumption and economic growth nexus: A long time span analysis. I*nternational Energy Journa*l 15: 143-150.

[4] IEA, I., UNSD, WB, 2019. WHO Tracking SDG 7: *The Energy Progress Report 2019*. Washington DC.

[5] Dejtrakulwong C. and S. Patumsawad. 2014. Four Zones Modeling of the Downdraft Biomass Gasification Process: Effects of Moisture Content and Air to Fuel Ratio. *Energy Procedia* 52: 142-149.

[6] Jaojaruek K., 2014. Mathematical model to predict temperature profile and air–fuel equivalence ratio of a downdraft gasification process. *Energy Conversion and Management* 83: 223-231.

[7] Susastriawan A.A.P., Saptoadi H., and Purnomo, 2017. Small-scale downdraft gasifiers for biomass gasification: A review. *Renewable and Sustainable Energy Reviews* 76: 989-1003.

[8] Basu P., 2018. *Chapter 8 - Design of Biomass Gasifiers, in Biomass Gasification, Pyrolysis and Torrefaction (Third Edition)*, P. Basu, Editor. Academic Press. p. 263-329.

[9] Shelke G. and P. Mahanta. 2015. Feasibility study on utilization of biomass briquette in a conventional downdraft gasifier. *International Energy Journal* 15(4): 157-166.

[10] Rubio M.G., and K. Jaojaruek. 2018. Small-scale shaking single-stage downdraft biomass gasifier. *International Energy Journal* 18(4): 321-330. doi:10.1109/COGEN.2016.7728949

[11] Kongkapisuth K., Roynarin W., and Intholo D., 2017. Study of building effects on small HAWTs performance in building - Obstructed wind flow area by using a CFD k-ϵ turbulence model validated with site measurement. *International Energy Journal* 17: 193-210.

[12] Khan I., Baruah M., Dewan A., and Mahanta P., 2009. Computational investigation of energy efficient pin fin cross section for a compact heat exchanger. *International Energy Journal* 10: 233-246.

[13] Silva J., Teixeira J., Teixeira S., Preziati S., and Cassiano J., 2017. CFD modeling of combustion in biomass furnace. *Energy Procedia* 120: 665-672. doi:10.1016/j.egypro.2017.07.179.

[14] Kumar U. and M.C. Paul. 2019. CFD modelling of biomass gasification with a volatile break-up approach. *Chemical Engineering Science*, 2019. 195: 413-422.

[15] Jaojaruek K., Jarungthammachote S., Gratuito M.K.B., Wongsuwan H., and Homhual S., 2011. Experimental study of wood downdraft gasification for an improved producer gas quality through an innovative two-stage air and premixed air/gas supply approach. *Bioresource Technology*, 102(7), 4834-4840. doi:https://doi.org/10.1016/j.biortech.2010.12.024.

[16] ANSYS, I., *ANSYS CFX-Solver Theory Guide*. 2017: Canonsburg, PA.

[17] Magoss E., 2008. *General Regularities of Wood Surface Roughness.* Acta Silvatica & Lignaria Hungarica, 4.

[18] Masmoudi M.A., Halouani K., and Sahraoui M., 2017. Comprehensive experimental investigation and numerical modeling of the combined partial oxidation-gasification zone in a pilot downdraft air-blown gasifier. *Energy Conversion and Management* 144: 34-52.

[19] James Rivas A., Yuan W.D., Boyette M., and Wang D., 2015. The effect of air flow rate and

biomass type on the performance of an updraft biomass gasifier. *BioResources 10*. doi:10.15376/biores.10.2.3615-3624.

[20] Luckos A. and J.R. Bunt. 2011. Pressure-drop predictions in a fixed-bed coal gasifier. *Fuel* 90(3): 917-921.

[21] Koekemoer A. and A. Luckos. 2015. Effect of material type and particle size distribution on pressure drop in packed beds of large particles: Extending the Ergun equation. *Fuel* 158: 232-238.